Article

Precise Determination of Magnetic Gradient Relaxation of Coupled Atomic Spin Ensemble in Spin-Exchange Relaxation-Free Co-Magnetometer

Xiujie Fang [1,2] , **Kai Wei** [1,2], **Wenfeng Fan** [1,2] , **Siran Li** [1,2,3,*] , **Qian Cao** [1,2,*], **Wei Quan** [1,2], **Yueyang Zhai** [1,2] **and Zhisong Xiao** [4]

1 Key Laboratory of Ultra-Weak Magnetic Field Measurement Technology, Ministry of Education, School of Instrumentation and Optoelectronic Engineering, Beihang University, Beijing 100191, China
2 Zhejiang Provincial Key Laboratory of Ultra-Weak Magnetic-Field Space and Applied Technology, Hangzhou Innovation Institute, Beihang University, Hangzhou 310051, China
3 The Shenyuan Honors College, Beihang University, Beijing 100191, China
4 School of Physics, Beihang University, Beijing 100191, China
* Correspondence: lsr2014@buaa.edu.cn (S.L.); buaacq@buaa.edu.cn (Q.C.)

Abstract: Inside a spin-exchange relaxation-free (SERF) co-magnetometer with a high-pressure buffer gas atomic cell, the magnetic field gradient causes the decoherence of atomic spins to produce magnetic-field gradient relaxation. This paper presents a new method for the accurate measurement of magnetic field gradient relaxation of alkali metal atoms and inert atoms of strongly coupled spin systems under triaxial magnetic field gradients in the K-Rb-^{21}Ne co-magnetometer. The magnetic field gradient relaxation of alkali metal atoms is measured using a step magnetic field modulation method, and the magnetic field gradient relaxation of inert atoms is measured using a combined free induction decay and spin growth method. The method does not require the use of large background magnetic fields and RF fields to maintain the atoms in the SERF state, does not require additional optics, and is not affected by the pumping or detecting of optical power. A kinetic model that considers a large electron-equivalent magnetic field was designed and a gradient relaxation model was developed. The quadratic coefficients of the experimentally measured gradient relaxation curves fit the theoretical model well over the range of the applied magnetic field gradients, confirming the validity of the proposed method.

Keywords: spin-exchange relaxation-free (SERF) co-magnetometer; magnetic field gradient relaxation; strongly coupled spin system

1. Introduction

The atomic spin inertial sensor has angular momentum based on the spin properties of the atom. It carries out Larmor precession in the presence of a magnetic field to achieve inertial measurement. It was developed based on the spin-exchange relaxation-free (SERF) effect proposed by the Happer team in 1973, in which the spin-exchange relaxation between atoms can be eliminated under high-temperature conditions with high-density atoms in a low magnetic environment [1,2]. The co-magnetometer can be divided into nuclear spin inertial measurements as inertial sensing carriers and ultrahigh-sensitive magnetometers as the final signal output to detect magnetic field signal probes. The ultrahigh-sensitive magnetometer has surpassed the superconducting quantum interference device by achieving a 0.16 fT/Hz$^{1/2}$ magnetic field measurement index [3,4]. The SERF co-magnetometer is an important development direction and research focus in the field of quantum precision measurements [5–8]. Current studies show that magnetic field gradient is an important factor affecting the performance improvement of co-magnetometers [9,10]. A magnetic field gradient produced by a light field, magnetic shield system, and temperature field exists

inside the device. In an atomic vapor cell with a high-pressure buffer gas, the magnetic field gradient causes atomic spin decoherence to produce magnetic field gradient relaxation. Incoherent precession results in the attenuation of the total spin polarization and an increase in the resonance line width [11]. Theoretical analysis and accurate measurement of the influence of the triaxial magnetic field gradient on magnetic-field gradient relaxation of hybrid atomic-coupled spin systems is key to improving the co-magnetometer sensitivity.

Several conventional measurement methods for the relaxation of alkali atoms in the SERF regime have been calculated using the resonance line width [12]. Most of these are based on the synchronous pumping technique [13] and electron paramagnetic resonance [14]. In the case of the synchronous pumping method, the original optical path of the device must be changed, additional optical modulators such as choppers are invoked to switch the pumping optical field, and relaxation parameters are measured according to the transient atomic response [15,16]. This method increases the complexity of the system and introduces additional noise. Additional application of a transverse RF field or a large background field is required using the electron paramagnetic resonance method. This is contrary to the condition that atoms in the SERF regime should be in an extremely weak magnetic environment. To measure the triaxial magnetic field gradient relaxation of pure alkali metal atoms, we proposed a fast spin-exchange interaction method that uses magnetic field excitation and amplitude spectrum analysis [17]. However, for the SERF co-magnetometer, the atomic source includes alkali metal atoms and noble atoms with long relaxation times. The alkali metal atoms are pumped-polarized and subsequently transfer the angular momentum to the inert atoms through spin-exchange collisions. This results in the hyperpolarization of the inert atoms, which are strongly coupled with the alkali metal atoms, and the above-mentioned atomic magnetic field gradient relaxation measurement method is no longer applicable.

Methods for measuring the relaxation of inert atoms include spin-flip, spin-growth [18], and free-induction decay (FID) methods [19]. The spin-flip method requires the reversal of polarization by using π pulses. This method requires additional optical elements to be introduced into the device, which increases the complexity of the experiment and reduces the measurement accuracy. The signal intensity of the state in which the unpolarized status of the coupled atomic system is synthesized and gradually reaches stability was measured using the spin-growth method. The free induction decay method was used to obtain the spin-decay curve by applying a magnetic field step modulation signal to record the signal amplitude. Because applying magnetic field modulation will affect the polarization of inert atoms, the measurement accuracy is not high using the FID method alone in the experiment. The above two methods are not affected by the pumped optical power and detected optical power and do not require the addition of external measurement equipment.

The objective of this study was to design an accurate measurement method for the magnetic gradient relaxation of alkali metal and inert atoms in the strongly coupled spin-system synthesis of the SERF co-magnetometer under triaxial gradient magnetic field conditions. The magnetic field gradient relaxation of alkali metal atoms is measured using a step magnetic field modulation method, and the magnetic field gradient relaxation of inert atoms is measured using a combined free induction decay and spin growth method. The method provides a measurement means for reducing the relaxation of the magnetic field gradient in coupled atomic systems and provides data support for enhancing the self-compensating capability of coupled atomic systems and further improving the sensitivity of co-magnetometers.

2. Basic Principle

2.1. Fundamentals of Co-Magnetometer

The atomic spin system in the K-Rb-^{21}Ne co-magnetometer includes light-pumping alkali metal electron spin processes and alkali metal electron spins hyperpolarizing inert nucleus spins through spin-exchange collisions. In co-magnetometers, the polarized noble gas atoms are the key working substance for the measurements. The start-up time of the

device is determined by the hyperpolarization time of the nuclear spins, and the degree of spin polarization of the inert atomic nuclei determines the dynamic range of the inertial measurements [8]. Electron spins of alkali metal atoms transfer photon energy to inert atomic nuclear spins through spin-exchange collisions. The inert nucleon polarization is low when the atomic density of the alkali metal is small, and increasing the atomic density of the alkali metal can further increase the inert nucleon polarization. When only a single alkali metal atom is present inside the gas chamber, the greater the atomic density and the greater the optical depth inside the chamber, the faster the optical decay of the pumped light, which not only reduces the efficiency of the hyperpolarized inert atoms but also brings about a large polarization gradient which affects the inertial measurement sensitivity. This problem is solved using a hybrid pumping technique, whereby two alkali metal atoms are charged into the gas chamber, one of which has a lower density and can be uniformly polarized by the pumping laser. The polarized low-density alkali metal atoms transfer their atomic spin uniformly to the high-density alkali metal via atomic spin-exchange collisions, and the polarized high-density alkali metal atoms then hyperpolarize the inert atoms by the spin-exchange optical pumping process [20].

For alkali metal atoms, the spin-collision cross-sectional area of the K atom is smaller than that of the Rb atom, but at the same experimental temperature, the saturated vapor temperature pressure density of the Rb atom is greater than that of the K atom, and the Rb atom reaches a higher density at lower experimental temperatures. The laser pumping of low-density K atoms and the polarization of high-density Rb atoms by spin-exchange collisions are therefore used for hybrid pumping [21].

Polarized alkali metal atomic spin ensembles have optical rotation properties. After the linearly polarized detection light synthesized by left-circularly polarized light and right-circularly polarized light, which is detuned to the resonance frequency, passes through the polarized atom vapor due to the birefringence effect, the polarization direction of the detected light changes. The angle of polarization change of the detected light incident along the x direction is proportional to the projection of alkali metal polarizability in the x direction. It is used to detect the magnetic field and rotation signal of the input device. The angle of rotation when the detection light is detected using the D1 line is [22]:

$$\theta = -\frac{\pi}{2} n_{Rb} l r_e c P_e f_{D1} \frac{v_{pr} - v_{D1}}{\left(v_{pr} - v_{D1}\right)^2 - \left(\Gamma_{D1}/2\right)^2},$$ (1)

where l is the interaction distance between the probe light and the alkali metal atom, n_{Rb} is the density number of the rubidium atom, c is the propagation speed of the light, r_e is the radius of the electron. Γ_{D1}, f_{D1}, and v_{D1} are the pressure width, oscillation intensity, and resonance frequency of the probe light on the Rb D1 line, respectively. v_{pr} is the frequency of the probe light.

In order to suppress low-frequency noise, a photoelastic modulator (PEM) is used to detect the light in the high-frequency band to improve the detection sensitivity. The PEM's modulation amplitude is α_m, and modulation frequency is ω_m. The amount of phase delay is $\delta(t) = \alpha_m \sin(\omega_m t)$. According to Marius' law and the principle of polarized light propagation, the light intensity received by the photodetector I_t is:

$$I_t = \left[\frac{I_0 \alpha_m^2}{8} + I_0 \theta \alpha_m \sin(\omega_m t) - \frac{I_0 \alpha_m^2}{8} \cos(2\omega_m t) \right],$$ (2)

I_0 is the initial light intensity into the vapor cell through the deflector. Finally, PD is used to convert the optical signal into an electrical signal. The final output V_{out} of the co-magnetometer is as follows:

$$V_{out} = \eta M_{ac} I_0 e^{-oD(v)} \alpha_m \theta,$$ (3)

where η is the conversion factor of PD, M_{ac} is preamplifier gain, and OD is the optical depth.

2.2. Dynamics Modeling of Spin Ensembles in Magnetic Fields

The density matrix can be used to describe the mathematical model of atomic-spin system synthesis under the combined effect of the magnetic field, rotation signal, and spin coupling system in the SERF co-magnetometer. However, its solution process is too complicated. The atoms are subjected to a notably small spin-in angle by the external environment, and the Bloch equations are simplified into a linearized matrix.

In this paper, based on the SERF co-magnetometer of the K-Rb-^{21}Ne atomic source, the alkali metal atoms K and Rb are indistinguishable from each other owing to the fast atomic-spin-exchange collision process, the polarization rates of K and Rb atoms, and the signals of their responses to the magnetic field being the same. The Bloch equations of the two atoms are combined to establish the equivalent K-Rb atomic mixing equation. In this equation, when the density ratio of K and Rb atoms is $D_r = n_K / n_{Rb}$, the equivalent equation is [23,24]:

$$R_p^{Rb} = \frac{D_r R_p^K}{1 + D_r},$$ (4)

$$R_{se}^{ne} = \frac{D_r R_{se}^{^{21}Ne-K} + R_{se}^{^{21}Ne-Rb}}{1 + D_r},$$ (5)

$$R_{se}^{en} = R_{se}^{K-^{21}Ne} + R_{se}^{Rb-^{21}Ne},$$ (6)

where R_p^{Rb} and R_p^K is the rate of pumping to Rb and K atoms, respectively; R_{se}^{ne}, R_{se}^{en} are the K-Rb to ^{21}Ne exchange-collision relaxation rate and ^{21}Ne to K-Rb exchange-collision relaxation rate, respectively. $R_{se}^{K-^{21}Ne}$ and $R_{se}^{Rb-^{21}Ne}$ are K to ^{21}Ne exchange-collision relaxation rate and Rb to ^{21}Ne exchange-collision relaxation rate, respectively.

When the pumping light is along the *z*-axis, and the probe light is along the *x*-axis, the equivalent set of Bloch equations for the mixed K-Rb atomic source with inert atom ^{21}Ne can be expressed as follows [23,25]:

$$\frac{\partial \vec{P^e}}{\partial t} = \frac{\gamma_e}{Q(P^e)} \left(\vec{B} + \lambda M_0^n \vec{P^n} \right) \times \vec{P^e} - \vec{\Omega} \times \vec{P^e} + \frac{R_p^{Rb} \vec{s_P} + R_{se}^{en} \vec{P^n}}{Q(P^e)} - \frac{\{R_1^e, R_2^e, R_2^e\} \vec{P^e}}{Q(P^e)},$$ (7)

$$\frac{\partial \vec{P^n}}{\partial t} = \gamma_n \left(\vec{B} + \lambda M_0^e \vec{P^e} \right) \times \vec{P^n} - \vec{\Omega} \times \vec{P^n} + R_{se}^{ne} \vec{P^e} - \{R_1^n, R_2^n, R_2^n\} \vec{P^n},$$ (8)

where P^n and P^e represent the electron and nuclear spin polarization of alkali metal and inert atoms, respectively; γ_n and γ_e represent the gyromagnetic ratio of the alkali metal and inert atoms, respectively; $Q(P^e)$ is the slowing factor for alkali metal atoms in the SERF regime; and B and Ω, respectively, denote the externally applied magnetic field and the angular velocity of rotation information. In addition, the direction of angular momentum transfer of the pumped photon is s_P; and R_1 and R_2 are the respective longitudinal and transverse relaxation rates of the atoms. Moreover, the equivalent magnetic fields engendered by the strongly joined coupling of alkali metal atoms and noble gas nuclei due to the interatomic Fermi contact interaction are $\lambda M_0^e P^e$ and $\lambda M_0^n P^n$, respectively. Equations M_0^e and M_0^n are the fully polarized magnetic moments of the alkali metal and inert atoms, respectively; λ is the enhancement factor for the Fermi contact interaction.

In the experimentally mixed atomic gas chamber, the density of inert atoms is much greater than that of the alkali metals, and the magnetic field generated by inert atoms is greater than the electron magnetic field. In a spherical atomic vapor cell, the enhancement factor for the Fermi contact interaction can be expressed as $\lambda = 2\kappa_0/3$, where κ_0 is the contact constant for the Fermi interaction between atoms. The κ_0 values for different atomic sources are listed in Table 1.

Table 1. Contact constants of Fermi interactions between different atomic sources.

| Atomic Source Type	Fermi Contact Constant
K-^{21}Ne	30.8 ± 2.7 [26]
K-^{4}He	5.99 ± 0.11 [27]
Rb-^{21}Ne	32.0 ± 2.9 [28]
Rb-^{4}He	6.39 ± 0.02 [28]
Rb-^{129}Xe	644 ± 269 [29]
Cs-^{129}Xe	653 ± 20 [30]

In our experiments using the large Fermi contact constant of Rb-^{21}Ne, the equivalent magnetic field generated by the alkali metal atoms cannot be neglected during the solution of the Bloch equation. When the transverse square-wave step magnetic fields ΔB_y and ΔB_x are input, the transverse polarization of the alkali metal atoms changes ΔP_x^e according to the steady-state solution of Equation (7) as

$$\frac{\Delta P_x^e}{\Delta B_y} = \frac{\left(\lambda M_0^n P_z^n - \delta B_z\right)\delta B_z P_z^e R_2^e \gamma_e}{\left(\lambda M_0^n P_z^n - \delta B_z\right)^2 R_2^{e\,2} + \left(\lambda M_0^e P_z^e + \lambda M_0^n P_z^n - \delta B_z\right)^2 \delta B_z^2 \gamma_e^2}, \tag{9}$$

$$\frac{\Delta P_x^e}{\Delta B_x} = \frac{\left(\lambda M_0^e P_z^e + \lambda M_0^n P_z^n - \delta B_z\right)\delta B_z^2 P_z^e \gamma_e^2}{\left(\lambda M_0^n P_z^n - \delta B_z\right)^2 R_2^{e\,2} + \left(\lambda M_0^e P_z^e + \lambda M_0^n P_z^n - \delta B_z\right)^2 \delta B_z^2 \gamma_e^2}. \tag{10}$$

In the above solution, δB_z is the residual magnetic field in the z-direction, and the expression is $\delta B_z = B_z - B_z^c$; B_z is the magnetic field applied in the z-direction; B_z^c is the working self-compensating point of the SERF co-magnetometer with the expression $B_z^c = \lambda M_0^e P_z^e + \lambda M_0^n P_z^n$. At the operating point B_z^c, the strongly coupled atomic spin system has a self-compensating feature that automatically compensates for the disturbing magnetic field noise introduced by the external environment. It has the best dynamic performance currently [31].

Figure 1 shows the output response curves of the device obtained using the transverse square-wave modulation method for different residual magnetic fields, δB_z, under simulated conditions.
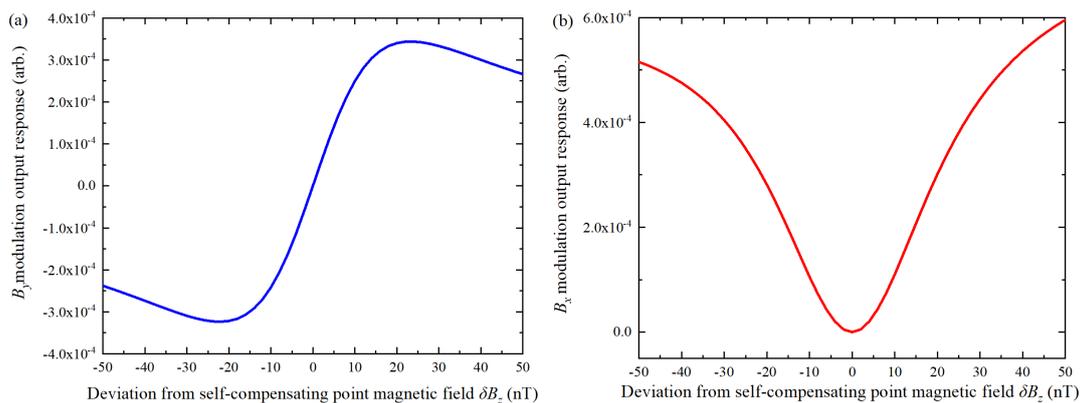
Figure 1. B_y and B_x step magnetic field modulation output response of SERF co-magnetometer. (**a**) B_y modulation output response at different residual magnetic fields. (**b**) B_x modulation output response at different residual magnetic fields.

By changing the residual magnetic field, δB_z, when applying B_x square-wave magnetic field modulation, the output response of the inertial device is an absorption curve line, and the output response is a Lorentzian line when modulated by a B_y square-wave magnetic field. The transverse relaxation parameters of the alkali metal atoms R_2^e in the strongly coupled atomic source can be obtained using Equations (9) and (10).

2.3. Magnetic Gradient Relaxation Theory for Coupled Atomic Spin Systems

Here, the alkali metal atomic relaxation rate and inert atomic relaxation rate in the SERF co-magnetometer system are discussed. For alkali metals, the atomic relaxation rates are divided into transverse and longitudinal relaxation rates, where the longitudinal relaxation rates of alkali metal atoms are composed as follows [32]:

$$R_1^e = \frac{1}{Q(P^e)}\left(R_{sd}^e + R_P + R_{pr}\right) + R_{wall}^e + R_{1\Delta B}^e, \tag{11}$$

where R_{sd}^e is the spin-destroying collisional relaxation, which occurs when there are collisions between alkali metal atoms, between alkali metal atoms and inert atoms, and between alkali metal atoms and buffer and quenching gases. R_{wall}^e is the collisional relaxation of alkali metal atoms colliding with the walls of the gas chamber, where the collision causes the atoms to incur decoherence and to relax rapidly. $R_{1\Delta B}^e$ is a longitudinal gradient relaxation of alkali metal atoms.

For the lateral relaxation of alkali metal atoms, the factors causing atomic spin precession decoherence act on the lateral relaxation, which is expressed as

$$R_2^e = R_1^e + R_{SE} + R_{2\Delta B}^e, \tag{12}$$

where R_{SE} is the spin-exchange collisional relaxation between atoms. $R_{2\Delta B}^e$ is a transverse gradient relaxation of alkali metal atoms.

When the alkali metal atomic density is high and, in a notably low magnetic field experimental environment, the spin-exchange collisional relaxation of alkali metal atoms can be suppressed or even eliminated when the spin-exchange collisional rate is much higher than the spin-Larmor feeding frequency of the alkali metal atoms in the SERF state. Alkali metal atoms in the SERF operating state exhibit a spin-temperature distribution with a spin-exchange relaxation rate expressed as [33]

$$R_{SE} = \frac{\gamma_e^2 B^2 (Q(P^e)^2 - (2I+1)^2)}{2Q(P^e)^2 R_{se}^e}. \tag{13}$$

Inside the inertial measurement device, the pumped optical field polarization rate gradient, the magnetic shielding static magnetic field gradient, and the residual magnetic field gradient of the heating system result in the decoherence of the atomic spins. The large value of the main magnetic field, the alkali metal atomic spin longitudinal magnetic field gradient relaxation, and the transverse magnetic field gradient relaxation are expressed as [17]

$$R_{1\Delta B}^e = 2D\frac{\left|\vec{\nabla} B_x\right|^2 + \left|\vec{\nabla} B_y\right|^2}{B_0^2}, \tag{14}$$

$$R_{2\Delta B}^e = \frac{8\gamma^{e2} r^4 \left|\vec{\nabla} B_z\right|^2}{175 D Q(P_z)^2}, \tag{15}$$

where B_0 is the value of the main magnetic field incurred by atoms on the *z*-axis, *r* is the radius of the atomic vapor cell, and *D* is the temperature- and pressure-dependent diffusion coefficients.

The ^{21}Ne noble atomic relaxation rate in the K-Rb-^{21}Ne co-magnetometer is

$$R_{rel}^n = R_{se}^{en} + R_{quad}^n + R_{sd}^n + R_{\Delta B}^n, \tag{16}$$

where R_{quad}^n is the electric quadrupole moment relaxation resulting from collisions between ^{21}Ne atoms, which is related to the atomic density. $R_{\Delta B}^n$ is the magnetic gradient relaxation term of ^{21}Ne in the magnetic field gradient, where the longitudinal magnetic field gradient

relaxation term is like those of the alkali metal atoms, and the transverse magnetic field gradient relaxation is the following [34,35]:

$$R_{1\Delta B}^n = 2D \frac{\left|\vec{\nabla} B_x\right|^2 + \left|\vec{\nabla} B_y\right|^2}{B_0^2}, \tag{17}$$

$$R_{2\Delta B}^n = \frac{8\gamma^{e2} r^4 \left|\vec{\nabla} B_z\right|^2}{175D}, \tag{18}$$

By means of the above-mentioned modeling of the dynamics of the strongly coupled atomic spin system and the relaxation model under magnetic field gradients, the magnetic gradient relaxation of alkali metal atoms and inert atoms was accurately measured. More specifically, a triaxial magnetic field gradient was applied through a gradient coil, and a step magnetic field modulation method and spin-growth method combined with the FID method were applied.

3. Experimental Setup

A diagram of the experimental setup is shown in Figure 2. The device is divided into four main subsystems: a sensitive head system, an electronic measurement and heating system, magnetic shielding and magnetic compensation system, and a pumping and probe light system. The sensitive head system is at the center of the unit and includes a mixed atomic vapor cell, a non-magnetic vacuum structure, and a water-cooled structure. A spherical vapor cell with a 6 mm radius contains K and Rb with a density ratio $Dr = 1:86$. The mixed alkali metal atomic density is $n_e = 7.51 \times 10^{13}$ cm^{-3}; 15 Torr N_2 is the quench gas, and 2080Torr ^{21}Ne. The atomic vapor cell is made of aluminosilicate glass. Non-magnetic materials are used inside the device to keep the atoms in extremely weak magnetic field experimental conditions, ensuring that the atoms are always in the SERF state. The non-magnetic vacuum structure is mainly used to ensure temperature stability so that the atomic parameters in the atomic gas chamber are fixed values and prevent uneven distribution of atomic density in the atomic gas chamber caused by temperature gradient generated by heating. The water-cooled part is wound around the outside of the vacuum cavity to reduce temperature, prevent the high temperature from affecting magnetic shielding and magnetic compensation performance, and avoid introducing new thermal magnetic noise.

The cells were placed in a ceramic oven controlled by a proportional-integral conductor at 80 kHz AC and heated to 190 °C. At the same time, in order to avoid generating additional magnetic field noise, the heating line is twisted to cancel the magnetic field of the heating coil. The cell temperature was monitored using a PT1000 resistor with a temperature control accuracy of ±5 mK. Insulation outside the oven was achieved with a non-magnetic polyether ether ketone vacuum cavity. The device required an extremely weak magnetic field condition—ensuring that the atoms were in a SERF state—using a magnetic shielding system with low magnetic noise and a high magnetic shielding factor [36,37]. The magnetic shielding system consisted of an outer layer of four μ-metals with a shielding factor of 10^5, as well as a residual field of 0.5 nT and a magnetic noise of 5 fT/Hz$^{1/2}$ inside the device after shielding [38]. A set of triaxial compensation coils with a set of triaxial gradient coils driven by a function generator (33500B, Keysight, Santa Rosa, CA, USA) was used.
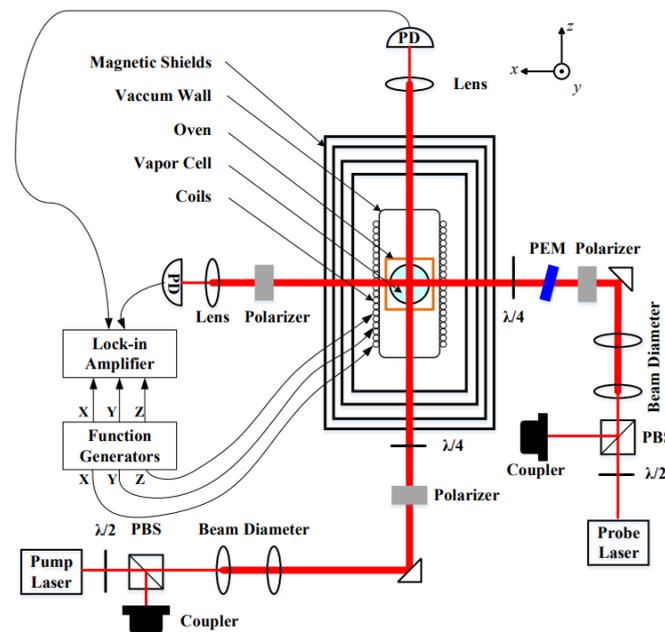
Figure 2. Experimental setup. $\lambda/4$: quarter-wave plate. $\lambda/2$: half-wave plate. PD: photodetector. PBS: polarized beam splitter. PEM: photoelastic modulator.

Both the pumping and probe lights were generated by the distributed Bragg reflector laser. The pumping laser was beaming split by a PBS, and one of the beams was used to monitor the laser wavelength. The beam radius was expanded to 7 mm by a lens beam spreading system and then passed through a quarter-wave to circularly polarize light for pumping the alkali metal atoms. The pumping power was 412 mW, and the wavelength was locked to the D1 line of the K atom at 770.107 nm. The probe light beam radius was 2 mm, the power was 11.3 mW, and the wavelength was 795.511 nm. It was detuned away from the D1 line of Rb atoms. To isolate low-frequency noise and improve the probe sensitivity, a photoelastic modulator (PEM) probe method was used. The PEM model used in the experiments was from I/FS Hinds Instruments with a modulation frequency of 50 kHz and a modulation angle of 0.08 rad. The co-magnetometer mainly focuses on low-frequency signals, so it needs to use a low-frequency non-magnetic vibration isolation device to isolate the vibration in the environment so that the vibration noise felt by the optical platform on the isolator is as small as possible.

Figure 2 shows the pumping light along the *z*-axis and the probe light along the *x*-axis. Polarized atomic spin ensembles exhibit optical rotation properties. After the linearly polarized probe light passes through the polarized atomic cell, the polarization direction of the probe light changes owing to the birefringence effect [39], where the refractive indices of the left- and right-handed polarized light are different. The angle of change in the polarization of the detection light incident along the *x*-direction is proportional to the projection of the alkali metal polarization rate in the *x*-direction for detecting the input device signal. The light rotation angle information is measured by a photodetector; the signal is amplified by a lock-in amplifier (HF2LI, Zurich Instruments, Zurich, Switzerland), and the optical signal is converted into a voltage signal. The voltage signal is then collected and processed using DAQ.

4. Results and Discussion

4.1. Magnetic Gradient Relaxation of Alkali Metal Atom Measurement

The residual magnetic field in the device was compensated with a DC magnetic field using triaxial compensation coils to identify the self-compensating operating point, where $\delta B_z = 0$. The magnetic gradient relaxation of alkali metal atoms in strongly coupled ensembles was measured. When no gradient magnetic field was applied, a step magnetic

field modulation was applied along the y-axis, the magnitude of the residual bias magnetic field δB_z value in the z-axis was changed, and the difference in the output signal response amplitude was measured. Accordingly, the transverse relaxation rate of the alkali metal atoms was measured according to Equation (9). From Equations (14) and (15), the transverse gradient magnetic field was related to the longitudinal magnetic gradient relaxation, and the longitudinal gradient magnetic field was related to the transverse magnetic gradient relaxation when the triaxial gradient magnetic field was applied separately. Equation (12) can be expressed as follows:

$$R_2^e = R_{1-0}^e + R_{SE} + R_{1\Delta B}^e + R_{2\Delta B}^e, \tag{19}$$

where R_{1-0}^e is the fixed relaxation value other than the spin-exchange relaxation rate, R_{SE} is the spin-exchange collisional relaxation between atoms before the triaxial magnetic field gradient is applied to the device. When no magnetic field gradient is applied, $R_{1\Delta B}^e = 0$, $R_{2\Delta B}^e = 0$.

The value of R_2^e can be obtained from the description in Section 2.2 by changing the residual magnetic field when applying square-wave magnetic field modulation. The slowing factor $Q(P^e)$ could be obtained by measuring the polarizability of alkali metal atoms in coupled spin ensembles based on the steady-state AC response [40], and the value of R_{SE} was calculated according to Equation (13). A fixed value of $R_{1-0}^e = R_2^e - R_{SE}$ was obtained according to the above steps. For the experimental measurements without magnetic field gradients, the transverse relaxation of the alkali metal atoms was at the self-compensating point $R_2^e = 4020.67 \text{ s}^{-1}$, the theoretical spin-exchange relaxation rate was $R_{SE} = 189.57 \text{ s}^{-1}$ with a fixed relaxation value $R_{1-0}^e = 3831.43 \text{ s}^{-1}$. The value of R_{1-0}^e was maintained constant in subsequent experiments with magnetic field gradients.

Subsequently, a triaxial magnetic field gradient ranging from 5 to 25 nT/cm was applied separately. The above steps were repeated to obtain an accurate measurement of the magnetic gradient relaxation of alkali metal atoms by measuring the transverse relaxation rate, measuring the slowing down factor, and calculating the spin-exchange relaxation rate. Figure 3 shows the difference between the highest and lowest output voltage of the device signal corresponding to the different residual magnetic field points of the step magnetic field modulation in the case of an applied magnetic field gradient along the z-axis and step-modulated magnetic field with amplitude 0.5 nT and frequency 0.2 Hz.
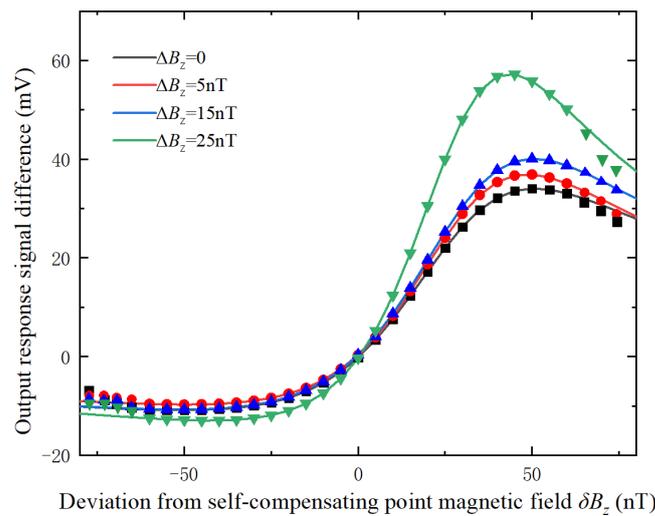
Figure 3. Experimental measurements of the stepped magnetic field modulated output response with an applied z-axis magnetic field gradient.

The results of the experimental measurements of the relaxation of the magnetic-field gradients of the alkali metal atoms in the applied x- and y-axis magnetic-field gradients are shown in Tables 2 and 3.

Table 2. Experimental results of magnetic gradient relaxation of alkali metal atoms in coupled spin ensemble under applied *x*-axis magnetic gradient.

Magnetic Field Gradient	5 nT/cm	10 nT/cm	15 nT/cm	20 nT/cm	25 nT/cm
R_2^e	4032.65 s^{-1}	4048.53 s^{-1}	4066.20 s^{-1}	4085.12 s^{-1}	4103.62 s^{-1}
R_{SE}	192.81 s^{-1}	208.91 s^{-1}	226.51 s^{-1}	244.77 s^{-1}	264.3 s^{-1}
$R_{1\Delta B_x}^e$	8.41 s^{-1}	8.13 s^{-1}	8.26 s^{-1}	8.92 s^{-1}	7.89 s^{-1}

Table 3. Experimental results of magnetic gradient relaxation of alkali metal atoms in coupled spin ensemble under applied *y*-axis magnetic gradient.

Magnetic Field Gradient	5 nT/cm	10 nT/cm	15 nT/cm	20 nT/cm	25 nT/cm
R_2^e	4051.22 s^{-1}	4069.02 s^{-1}	4072.18 s^{-1}	4089.65 s^{-1}	4094.43 s^{-1}
R_{SE}	160.57 s^{-1}	175.06 s^{-1}	183.20 s^{-1}	193.51 s^{-1}	204.96 s^{-1}
$R_{1\Delta B_x}^e$	59.22 s^{-1}	62.53 s^{-1}	57.55 s^{-1}	62.71 s^{-1}	58.04 s^{-1}

As observed in the above table, when only the transverse magnetic field gradient is applied, the relaxation of the magnetic field gradient of the alkali metal atoms does not change over the range of the applied magnetic field gradient. In the SERF co-magnetometer, both the alkali metal atoms and inert atoms experience the equivalent magnetic field generated by the atoms themselves in the self-compensating operating state owing to Fermi interactions for large main magnetic field conditions. According to Equation (14), in the range of 5 nT/cm to 25 nT/cm of transverse magnetic field gradients, the relaxation time of the magnetic-field gradient of the alkali metal atoms is on the order of milliseconds for this relaxation term to be undetectable.

The experimental measurements of the magnetic gradient relaxation with the *z*-axis magnetic field gradient applied alone are shown in Figure 4. The measured value is larger than the theoretical value owing to an increase in the longitudinal magnetic field gradient value along a quadratic curve. Here, the theoretical value quadratic coefficient is 0.0459, the experimental value quadratic coefficient is 0.0444, and the experimental measurement gradient relaxation changes in line with the theory, proving the correctness and validity of the proposed method.
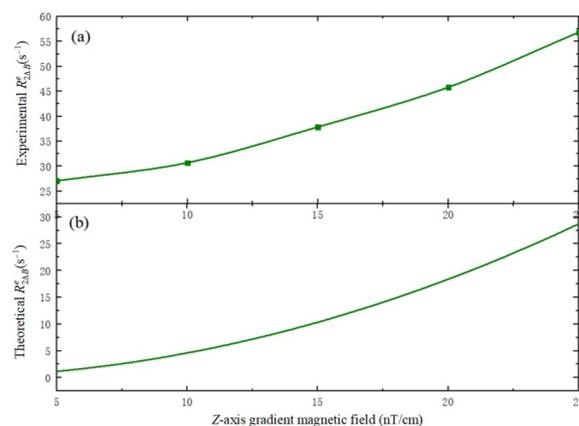
Figure 4. Experimental results of magnetic gradient relaxation of alkali metal atoms in coupled spin ensemble under applied *z*-axis magnetic gradient. (**a**) The experimental measurement results; (**b**) The simulation results based on the theoretical Equation (15).

4.2. Magnetic Gradient Relaxation of Inert Atom Measurement

The experimental measurements of the relaxation of the magnetic field gradient of inert atoms in a strongly coupled atomic system are presented below. The Bloch equation for inert atoms shows that when a transverse step magnetic field is applied, the solution to Equation (8) is:

$$P_x^n = P_z^n e^{-tR_2^n} \sin(\gamma^n B_0 t), \tag{20}$$

$$P_z^n = P_{z0}^n \left[1 - e^{-tR_{11}^n} \left(1 - \frac{P_{z0}^n}{P_0^n} \right) \right], \tag{21}$$

where t is the measurement time and P_0^n is the initial polarization rate of the inert atom is:

$$P_{z0}^n = \frac{R_{se}^{en}}{R_{se}^{en} + R_{rel}^n} P^e, \tag{22}$$

The above equation facilitates the measurement of the transverse and longitudinal relaxation rates of inert atoms using the FID method combined with the spin growth method. The inert atoms are coupled to the alkali metal atoms by hyperfine interactions, and the polarized noble gas atoms generate an equivalent magnetic field acting on the alkali metal atoms so that the incoming ^{21}Ne atoms can be detected by the in-situ atomic magnetometer composed of Rb atoms, which causes a change in the output signal of the co-magnetometer. The main magnetic field in the experiment is the value of the magnetic field at the self-compensating operating point, the step magnetic field is applied along the y-axis, and the device output signal and output amplitude fitting equations are:

$$S(t) = A \sin(\omega_0 t) e^{-tR_2^n} + S_0, \tag{23}$$

$$A(t_{pump}) = k \left(1 - e^{-t_{pump} R_1^n} \right), \tag{24}$$

where S_0 is the output signal bias, t_{pump} is the optical pumping time, and k is the scaling factor related to the initial polarization rate of the inert atoms. Figure 5 shows the experimental measurement of R_2^n of the inert atom without an applied magnetic field gradient. The experimental measurements fit the theoretical equation curve well, with a fit factor greater than 0.994, and the transverse relaxation of the inert atom without the applied magnetic field gradient is 0.065 s^{-1}.
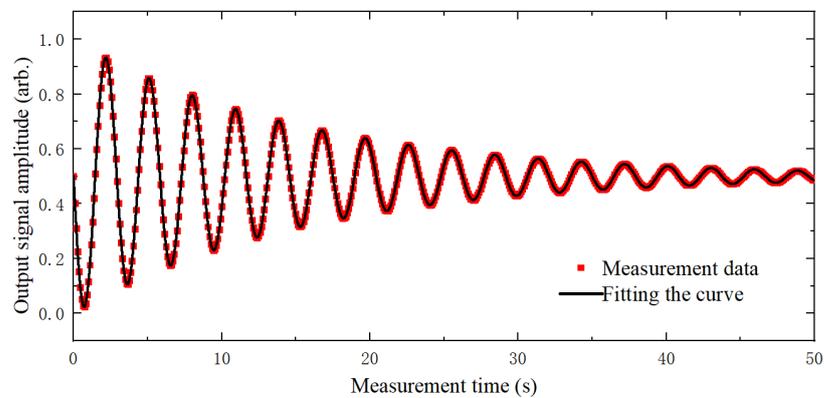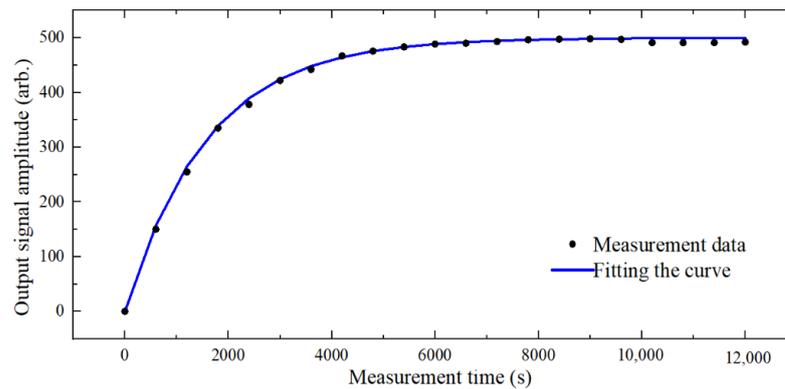

Figure 5. Experimental measurement of transverse relaxation rate of inert atoms in strongly coupled spin ensemble without magnetic field gradient.

This method, combined with the spin growth method, enables both the measurement of the transverse relaxation rate of inert atoms and the measurement of the R_1^n of inert atoms. According to Equations (20) and (21), the output signal amplitude in the measured FID

curve is related to the polarization rate and the initial polarization rate of inert atoms, and R_1^n of inert atoms is obtained from the relationship between the output signal amplitude and the optical pumping time.

The experimental procedure involved recording the amplitude values at regular intervals after the pumping light was switched on and until the polarization of the inert nuclei was completed. Figure 6 shows the results of the R_1^n measurements of inert atoms in the inertial atomic system. R_1^n of the inert atoms without application of the gradient coil is 0.00063 s^{-1}, which is a larger value than the R_{quad}^n from the collisions between the ^{21}Ne atoms calculated using the theoretical equation. This finding indicates the existence of gradient relaxation due to the transverse magnetic field gradient inside the device.

Figure 6. Experimental measurement of longitudinal relaxation rate of inert atoms in strongly coupled spin ensemble without magnetic field gradient.

The magnetic field gradient relaxation could then be accurately measured by applying a triaxial magnetic field gradient separately in the device and measuring the change in the transverse and longitudinal relaxation rates of the inert atoms using the method described above. Table 4 shows the measured R_2^n and R_1^n when the x-, y-, and z-axis magnetic field gradients were applied separately.

Table 4. Experimental results of R_2^n and R_1^n when the x-, y-, and z- axis magnetic field gradients are applied separately.

| Magnetic Field Gradient (x-axis)	5 nT/cm	10 nT/cm	15 nT/cm	20 nT/cm	25 nT/cm
R_2^n	0.0660 s^{-1}	0.0678 s^{-1}	0.0650 s^{-1}	0.0661 s^{-1}	0.0659 s^{-1}
R_1^n	0.000826 s^{-1}	0.00104 s^{-1}	0.00128 s^{-1}	0.000158 s^{-1}	0.000189 s^{-1}
Magnetic Field Gradient (y-axis)	**5 nT/cm**	**10 nT/cm**	**15 nT/cm**	**20 nT/cm**	**25 nT/cm**
R_2^n	0.0682 s^{-1}	0.0686 s^{-1}	0.070 s^{-1}	0.0682 s^{-1}	0.0679 s^{-1}
R_1^n	0.000864 s^{-1}	0.00107 s^{-1}	0.00133 s^{-1}	0.000159 s^{-1}	0.000196 s^{-1}
Magnetic Field Gradient (z-axis)	**5 nT/cm**	**10 nT/cm**	**15 nT/cm**	**20 nT/cm**	**25 nT/cm**
R_2^n	0.128 s^{-1}	0.151 s^{-1}	0.179 s^{-1}	0.208 s^{-1}	0.242 s^{-1}
R_1^n	0.000639 s^{-1}	0.000641 s^{-1}	0.000648 s^{-1}	0.000657 s^{-1}	0.000638 s^{-1}

It is clear from the measurements that R_2^n is almost constant when the x-axis and y-axis magnetic field gradients are applied separately, and that R_1^n is constant when the z-axis magnetic field gradient is applied alone.

Section 4.2 and Figure 8 show the experimental measurements of the longitudinal magnetic gradient relaxation time of inert atoms $R_{1\Delta B}^n$ when the x- and y-axis magnetic

field gradients are applied separately, the transverse magnetic gradient relaxation time of inert atoms $R_{2\Delta B}^n$ when the z-axis magnetic field gradients are applied alone, and the curves calculated by the theoretical formula.
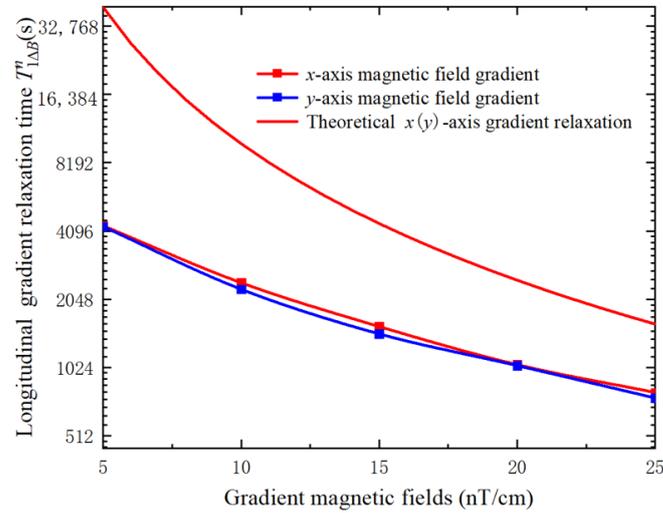
Figure 7. Measured relaxation times of the longitudinal magnetic gradient of inert atoms with an applied x- and y-axis magnetic field gradient, respectively, and curves calculated by the theoretical equations.
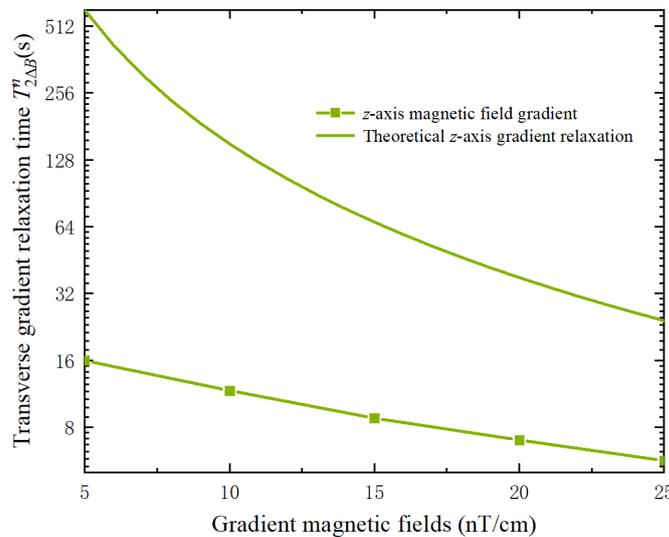
Figure 8. Measured relaxation times of transverse magnetic field gradients of inert atoms with z-axis magnetic field gradients applied alone and curves calculated from theoretical equations.

From the above experimental results, the quadratic coefficients of the longitudinal and transverse magnetic field gradient relaxation rate variation curves were 1×10^{-6} and 7×10^{-5}, respectively, and the variation patterns and magnitudes were the same as those of the theoretical model. The experimental measurement of the relaxation time was considerably lower than the value calculated by the theoretical equation. The theoretical values are calculated using a triaxial gradient magnetic field applied in the range of 5 nT/cm to 25 nT/cm. Before the application of the gradient coil, the inherent magnetic field gradient in the x- and y-axes inside the co-magnetometer was 5–10 nT/cm, and the inherent magnetic field gradient in the z-axis of the device was 20–25 nT/cm. In addition, in the measurement environment, the electrical heating system, the coupling of the coils, and the mutual coupling between the coils and the magnetic shield can generate other order

gradients of magnetic fields. Improving the linearity of the compensation and magnetic field gradient coils can further improve the accuracy of the proposed measurement method.

5. Conclusions

In this paper, precise measurements and analyses of the magnetic gradient relaxation of strongly coupled spin-system-synthesized alkali metal atoms and inert atoms in the SERF co-magnetometer under a triaxial magnetic field gradient were presented. In this study, a kinetic model for the large electron equivalent magnetic field of alkali metal atoms was developed and solved. A model for the relaxation of the magnetic field gradient of a coupled atomic system was developed. The magnetic gradient relaxation of alkali metal atoms was measured using the device response to the step magnetic field modulation method, and the magnetic gradient relaxation of inert atoms was measured using a combination of FID and spin-growth methods.

The proposed method does not require the application of a large background magnetic field, and it changes the optical path with additional optics. The atoms are guaranteed to be in the SERF state, and the measurements are independent of the pumping and detection powers. The experimental quadratic coefficient of magnetic field gradient relaxation for alkali metal atoms was 0.0444, and the theoretical quadratic coefficient was 0.0459 over the range of applied magnetic field gradients. The quadratic coefficients of the longitudinal and transverse magnetic field gradient relaxation variation curves measured experimentally for inert atoms were 1×10^{-6} and 7×10^{-5}, respectively, which well aligned with the theoretical model. The validity of the proposed method was thus confirmed. The experimental results demonstrated that, in the SERF co-magnetometer, the longitudinal magnetic field gradient acts mainly on the transverse magnetic gradient relaxation of the alkali metal and inert atoms, and the transverse magnetic gradient acts mainly on the longitudinal magnetic gradient relaxation of the inert atoms. Based on the research presented herein, we suggest the design of new methods to suppress the magnetic field gradient in the SERF co-magnetometer to improve its dynamic performance and sensitivity. This will be the focus of future research.

Author Contributions: Conceptualization, X.F. and S.L.; methodology, K.W.; validation, X.F., Q.C., W.F. and S.L.; formal analysis, X.F.; investigation, X.F. and S.L.; data curation, X.F.; writing—original draft preparation, X.F.; writing—review and editing, Q.C. and W.F.; project administration, W.Q., Y.Z. and Z.X.; funding acquisition, W.Q. and W.F. All authors have read and agreed to the published version of the manuscript.

Institutional Review Board Statement: Not applicable.

Informed Consent Statement: Not applicable.

Data Availability Statement: The data presented in this study are available on reasonable request from the corresponding author.

Conflicts of Interest: The authors declare no conflict of interest.

References

1. Happer, W.; Tam, A.C. Effect of rapid spin exchange on the magnetic-resonance spectrum of alkali vapors. *Phys. Rev. A.* **1977**, *16*, 5. [CrossRef]
2. Meyer, D.; Larsen, M. Nuclear Magnetic Resonance Gyro for Inertial Navigation. *Gyroscopy Navig.* **2014**, *5*, 75. [CrossRef]
3. Kominis, I.K.; Kornack, T.W.; Allred, J.C.; Romalis, M.V. A Subfemtotesla Multichannel Atomic Magnetometer. *Nature* **2003**, *422*, 596. [CrossRef] [PubMed]
4. Dang, H.B.; Maloof, A.C.; Romalis, M.V. Ultrahigh Sensitivity Magnetic Field and Magnetization Measurements with an Atomic Magnetometer. *Appl. Phys. Lett.* **2010**, *97*, 151110. [CrossRef]

5.   Larsen, M.; Bulatowicz, M. Nuclear Magnetic Resonance Gyroscope for DARPA's Micro-Technology for Positioning, Navigation and Timing Program. In Proceedings of the 2014 International Symposium on Inertial Sensors and Systems (ISISS), Laguna Beach, CA, USA, 25–26 February 2014; p. 1.

6.   Stoner, R.; Walsworth, R. Atomic physics: Collisions give sense of direction. *Nat. Phys.* **2006**, *2*, 17. [CrossRef]

7.   Fang, J.C.; Qin, J. Advances in Atomic Gyroscopes: A View from Inertial Navigation Applications. *Sensors* **2012**, *12*, 6331. [CrossRef]

8.   Zhao, T.; Ying, Y.; Wei, K.; Xie, H.T.; Mu, T.J.; Fang, X.J.; Xu, Z.T.; Zhai, Y.Y. Ultra-sensitive all-optical comagnetometer with laser heating. *J. Phys. D* **2022**, *55*, 165103. [CrossRef]

9.   Wei, K.; Zhao, T.; Fang, X.J.; Xu, Z.T.; Liu, C.; Cao, Q.; Wickenbrock, A.; Hu, Y.H.; Ji, W.; Fang, J.C.; et al. Ultrasensitive Atomic Comagnetometer with Enhanced Nuclear Spin Coherence. *Phys. Rev. Lett.* **2023**, *130*, 63201. [CrossRef]

10. Pang, H.Y.; Liu, F.; Fan, W.F.; Wu, Z.H.; Yuan, Q.; Quan, W. Comprehensive analysis of the effects of magnetic fieldgradient on the performance of the SERF co-magnetometer. *Opt. Express* **2023**, *31*, 5215. [CrossRef]

11. Schearer, L.D.; Walters, G.K. Nuclear Spin-Lattice Relaxation in the Presence of Magnetic-Field Gradients. *Phys. Rev. J.* **1965**, *139*, 1398. [CrossRef]

12. Happer, W.; Tang, H. Spin-exchange shift and narrowing of magnetic resonance lines in optically pumped alkali vapors. *Phys. Rev. Lett.* **1973**, *31*, 273. [CrossRef]

13. Allred, J.C.; Lyman, R.N.; Kornack, T.W.; Romalis, M.V. High-sensitivity atomic magnetometer unaffected by spin-exchange relaxation. *Phys. Rev. Lett.* **2002**, *89*, 130801. [CrossRef]

14. Ding, Z.C.; Long, X.W.; Yuan, J.; Fan, Z.F.; Luo, H. Sensitive determination of the spin polarization of optically pumped alkali-metal atoms using near-resonant light. *Sci. Rep.* **2016**, *6*, 32605. [CrossRef]

15. Li, R.J.; Quan, W.; Fang, J.C. Polarization Measurement of Cs Using the Pump Laser Beam. *IEEE Photonics J.* **2017**, *9*, 1. [CrossRef]

16. Ma, Y.N.; Zhang, K.X.; Wang, Y.G.; Yang, K.; Zhai, Y.Y.; Lu, J.X. Fast extraction of the electron spin-relaxationrate in the SERF magnetometer from a transient response. *Opt. Express* **2022**, *30*, 17383. [CrossRef]

17. Fang, X.J.; Wei, K.; Zhai, Y.Y.; Zhao, T.; Chen, X.; Zhou, M.T.; Liu, Y.; Ma, D.Y.; Xiao, Z.S. Analysis of effects of magnetic field gradient on atomic spin polarization and relaxation in optically pumped atomic magnetometers. *Opt. Express* **2022**, *30*, 3926. [CrossRef]

18. Mirijanian, J.J. Techniques to Characterize Vapor Cell Performance for a Nuclear-Magnetic-Resonance Gyroscope. Ph.D. Thesis, California Polytechnic State University, San Luis Obispo, CA, USA, 2012.

19. Savukov, I.M.; Romalis, M.V. NMR Detection with an Atomic Magnetometer. *Phys. Rev. Lett.* **2005**, *94*, 123001. [CrossRef]

20. Zhao, T.; Zhai, Y.Y.; Liu, C.; Xie, H.T.; Cao, Q.; Fang, X.J. Spin polarization characteristics of hybrid optically pumped comagnetometers with different density ratios. *Opt. Express* **2021**, *30*, 15. [CrossRef]

21. Li, Y.; Liu, X.J.; Cai, H.W.; Ding, M.; Fang, J.C. Optimization of the alkali-metal density ratio in a hybrid optical pumping atomic magnetometer. *Meas. Sci. Technol.* **2019**, *30*, 15005. [CrossRef]

22. Duan, L.H.; Fang, J.C.; Li, R.J.; Jiang, L.W.; Ding, M.; Wang, W. Light intensity stabilization based on the second harmonic of the photo elastic modulator detection in the atomic magnetometer. *Opt. Express* **2015**, *23*, 32481. [CrossRef]

23. Fang, J.C.; Chen, Y.; Lu, Y.; Quan, W.; Zou, S. Dynamics of Rb and ^{21}Ne spin ensembles interacting by spin exchange with a high Rb magnetic field. *J. Phys. B At. Mol. Opt. Phys.* **2016**, *49*, 135002. [CrossRef]

24. Chen, Y.; Quan, W.; Zou, S.; Lu, Y.; Duan, L.H.; Li, Y.; Zhang, H.; Ding, M.; Fang, J.C. Spin exchange broadening of magnetic resonance lines in a high-sensitivity rotating K-Rb-^{21}Ne comagnetometer. *Sci. Rep.* **2016**, *6*, 36547. [CrossRef] [PubMed]

25. Kornack, T.W.; Ghosh, R.K.; Romalis, M.V. Nuclear spin gyroscope based on an atomic comagnetometer. *Phys. Rev. Lett.* **2005**, *95*, 230801. [CrossRef] [PubMed]

26. Ghosh, R.K. Spin Exchange Optical Pumping of Neon and Its Applications. Ph.D. Thesis, Princeton University, Princeton, NJ, USA, 2009.

27. Babcock, E.; Nelson, I.A.; Kadlecek, S.; Walker, T.G. ^{3}He Polarization-Dependent EPR Frequency Shifts of Alkali-Metal–^{3}He Pairs. *Phys. Rev. A* **2005**, *71*, 13414. [CrossRef]

28. Stoner, R.E.; Walsworth, R.L. Measurement of the 21Ne Zeeman Frequency Shift Due to Rb-^{21}Ne Collisions. *Phys. Rev. A* **2002**, *66*, 32704. [CrossRef]

29. Schaefer, S.R.; Cates, G.D.; Chien, T.R.; Gonatas, D.; Happer, W.; Walker, T.G. Frequency Shifts of the Magnetic-Resonance Spectrum of Mixtures of Nuclear Spin-Polarized Noble Gases and Vapors of Spin-Polarized Alkali-Metal Atoms. *Phys. Rev. A* **1989**, *39*, 5613. [CrossRef]

30. Fang, J.C.; Wan, S.-A.; Chen, Y. Measurement of ^{129}Xe Frequency Shift Due to Cs-^{129}Xe Collisions. *Chin. Phys. B* **2014**, *23*, 63401. [CrossRef]

31. Wei, K.; Zhao, T.; Fang, X.J.; Li, H.R.; Zhai, Y.Y.; Han, B.C.; Quan, W. Simultaneous Determination of the Spin Polarizations of Noble-Gas and Alkali-Metal Atoms Based on the Dynamics of the Spin Ensembles. *Phys. Rev. A* **2020**, *13*, 44027. [CrossRef]

32. Seltzer, S.J. Developments in Alkali-Metal Atomic Magnetometry. Ph.D. Thesis, Princeton University, Princeton, NJ, USA, 2008.

33. Kornack, T.W.; Romalis, M.V. Dynamics of Two Overlapping Spin Ensembles Interacting by Spin Exchange. *Phys. Rev. Lett.* **2002**, *89*, 253002. [CrossRef]

34. Cates, G.D.; Schaefer, S.R.; Happer, W. Relaxation of spins due to field inhomogeneities in gaseous samples at low magnetic field and low pressures. *Phys. Rev. A* **1988**, *37*, 2877. [CrossRef]

35. Hasson, K.C.; Cates, G.D.; Lerman, K.; Bogorad, P.; Happer, W. Spin relaxation due to magnetic-field inhomogeneities: Quartic dependence and diffusion-constant measurements. *Phys. Rev. A* **1990**, *42*, 5766. [CrossRef]

36. Lu, J.X.; Zhang, S.W.; Zhou, Y.; Yan, Y.G.; Lu, F.; Wang, K.; Zhai, Y.Y.; Ye, M. Optimal buffer gas pressure in dual-beam spin-exchange relaxation-free magnetometers. *Sens. Actuator A Phys.* **2022**, *347*, 113928. [CrossRef]

37. Yan, Y.G.; Lu, J.X.; Zhang, S.W.; Lu, F.; Yin, K.F.; Wang, K.; Zhou, B.Q.; Liu, G. Three-axis closed-loop optically pumped magnetometer operated in the SERF regime. *Opt. Express* **2022**, *30*, 18300. [CrossRef]

38. Ma, D.Y.; Lu, J.X.; Fang, X.J.; Yang, K.; Wang, K.; Zhang, N.; Han, B.C.; Ding, M. Parameter modeling analysis of a cylindrical ferrite magnetic shield to reduce magnetic noise. *IEEE Trans. Ind. Electron.* **2022**, *69*, 991. [CrossRef]

39. Budker, D.; Gawlik, W.; Kimball, D.F.; Weis, A. Resonant nonlinear magneto-optical effects in atoms. *Rev. Mod. Phys.* **2002**, *74*, 1153. [CrossRef]

40. Lu, Y.; Zhai, Y.; Fan, W.; Zhang, Y.; Xing, L.; Jiang, L.W.; Quan, W. Nuclear magnetic field measurement of the spin-exchange optically pumped noble gas in a self-compensated atomic comagnetometer. *Opt. Express* **2020**, *28*, 17683. [CrossRef]